

Towards the end of drying of granular materials: enhanced evaporation and drying-induced collapse

Zhongzheng Wang¹, Benjamin Maillet², Jean-Michel Pereira³, and Yixiang Gan⁴

¹The University of Sydney

²Laboratoire Navier

³Ecole des Ponts ParisTech

⁴University of Sydney

November 26, 2022

Abstract

We experimentally study the drying of loosely packed wet glass beads at low initial water content. The drying rate is found to decrease at the start, corresponding to the decreasing rate period controlled by vapor diffusion, followed by a deviation in drying rate from the diffusion limited evaporation. The propagation of drying front associated with a sharp saturation gradient is identified through both image analysis and magnetic resonance imaging technique. The drying-induced collapse of granular medium is observed and quantified. The concentrated collapse at the end of drying suggests the existence of liquid in the form of liquid bridges in the apparent dry region until the end of drying process. Collapse event is found to be local, i.e., a clear boundary can be identified for each collapse event, below which the loosely packed medium remains intact. This indicates the existence of a saturation gradient in the apparent dry region. The drying dynamics and collapse statistics suggest that the observed transition of drying regimes is due to Kelvin effect. This work demonstrates for the first time the drying enhancement phenomenon due to Kelvin effect even for grains with size of hundreds of micrometers, and provides insights on the drying process of partially saturated granular materials, especially near the final period of evaporation.

Towards the end of drying of granular materials: enhanced evaporation and drying-induced collapse

Zhongzheng Wang^{a,b}, Benjamin Maillet^b, Jean-Michel Pereira^{b,*}, Yixiang Gan^{a,c,*}

^a*School of Civil Engineering, The University of Sydney, NSW 2006, Australia*

^b*Navier, Ecole des Ponts, Univ Gustave Eiffel, CNRS, Marne-la-Vallée, France*

^c*The University of Sydney Nano Institute, The University of Sydney, NSW 2006, Australia*

Abstract

We experimentally study the drying of loosely packed wet glass beads at low initial water content. The drying rate is found to decrease at the start, corresponding to the decreasing rate period controlled by vapor diffusion, followed by a deviation in drying rate from the diffusion limited evaporation. The propagation of drying front associated with a sharp saturation gradient is identified through both image analysis and magnetic resonance imaging technique. The drying-induced collapse of granular medium is observed and quantified. The concentrated collapse at the end of drying suggests the existence of liquid in the form of liquid bridges in the apparent dry region until the end of drying process. Collapse event is found to be local, i.e., a clear boundary can be identified for each collapse event, below which the loosely packed medium remains intact. This indicates the existence of a saturation gradient in the apparent dry region. The drying dynamics and collapse statistics suggest that the observed transition of drying regimes is due to Kelvin effect. This work demonstrates for the first time the drying enhancement phenomenon due to Kelvin effect even for grains with size of hundreds of micrometers, and provides insights on the drying process of partially saturated granular materials, especially near the final period of evaporation.

*Corresponding author

Email addresses: jean-michel.pereira@enpc.fr (Jean-Michel Pereira),
yixiang.gan@sydney.edu.au (Yixiang Gan)

Keywords: Evaporation, drying, granular material, porous media, liquid bridge, MRI

Highlights

- Drying-induced collapse of loosely packed granular media is observed and quantified.
- NMR technique is used to reveal the distribution of liquid during evaporation.
- The existence of liquid in the apparent dry region is evidenced by the concentrated collapse near the end of drying experiment.
- The enhancement of evaporation rate is observed and explained by Kelvin effect.

10 1. Introduction

Drying of porous media is essential in relation with many applications, such as food processing, drugs and cosmetics synthesis in the pharmaceutical industries, oil recovery, and soil treatment in agriculture. The basic mechanisms of drying of saturated porous media have been identified as two distinguishable stages [1–8]. In the first stage, although the primary drying front (below which the medium is saturated) is receding into the medium, the evaporation of liquid at the surface is constantly being supplied through capillary flow, leading to a constant evaporation rate, which is limited by the external conditions (i.e, velocity and relative humidity of surrounding air), until either a critical surface water content [3] or a characteristic depth [5] is reached. Then, the evaporation enters the second stage, and the drying rate starts to decrease as a result of dominance of vapor diffusion, which is accompanied by the secondary drying front (separating the dry region and capillary flow region) receding into the porous media [2, 6–9]. A schematic showing the drying process of porous media is shown in Fig. 1. Efforts have been made to predict this transition mainly through the force balance among capillary, viscous, and gravitational forces, depending on properties of liquid and solid matrix, such as surface tension, viscosity, wettability, and pore size distribution [2, 3, 5–9]. Nevertheless, most existing studies focused on the drying process of initially saturated porous media, and the drying of partially saturated media with low liquid content, especially towards the extreme end of drying, remains relatively unexplored.

For porous media at low water content, i.e, in the pendular state [10–12], water exists mainly in the form of liquid bridges, making the granular material cohesive as a result of the capillary force from liquid bridges [10, 12–15]. As a result, studies have demonstrated a significant decrease in packing fraction of wet porous media compared with dry (or fully saturated) media [16–19]. This may have several implications for the dynamics of drying processes. Firstly, as reported in the literature, for cohesionless particles with size typically greater than 100 μm (negligible van der Waals forces), the lower limit of packing fraction

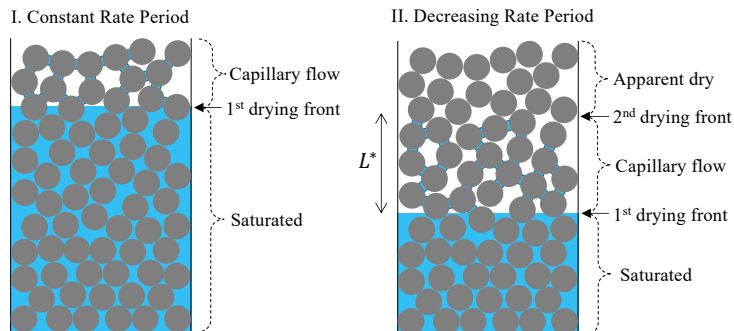


Figure 1: Schematic showing the drying process of porous media. In the constant rate period, evaporation of liquid at surface is supplied by capillary flow. After reaching a characteristic length L^* , the second drying front starts receding into the medium, marking the transition towards decreasing rate period.

40 is around 0.55 (random very loose packing) [20–24]. Therefore, drying-induced collapse may occur in loosely packed wet granular materials (e.g., packing fraction less than 0.55 for mono-sized spheres) as the liquid bridges disappear during evaporation. Besides, since the liquid bridges can be regarded as isolated in the pendular regime, the initial drying stage is expected to be fundamentally different from the saturated case where the connected liquid network can supply liquid towards the medium surface through capillary flow. Particularly, several studies have suggested that, apart from capillary flow, the film flow at grain surface due to adsorption can maintain the connectivity of liquid phase [25–28]. It is thus interesting to examine the potential influence of film flow on the drying process, especially at low initial water content.

In this work, we experimentally investigate the drying of loosely packed wet glass beads at low initial volumetric water content ($\sim 2\%$). Such low initial water is chosen in order to focus on the drying process near the end of drying, which also allows the generation of loosely packed sample and investigation on the drying-induced collapse. The sample was firstly prepared with desired packing fraction (~ 0.45) through a recently reported experimental procedure [11, 19], after which the drying experiment was conducted. The statistics of collapse events during drying as well as the evolution of liquid distribution

were obtained through image analysis and magnetic resonance imaging (MRI) technique, which provide global and local insights on physical mechanisms that govern the drying process.

2. Experiments

Materials and sample preparation: Mono-sized glass beads of average diameter $375.5 \mu\text{m}$ (standard deviation $31.8 \mu\text{m}$) are chosen with consideration of (1) to exclude the effect from van der Waals forces on packing structure, and (2) to have significant decrease in packing fraction once water is added [11, 16–19]. The sample was mixed thoroughly with water at volumetric water content $5 \pm 1\%$ [11, 19, 29]. Then, a sieve containing the wet glass beads was shaken by a vibration machine. A cylindrical container with inner diameter 13.70 ± 0.01 mm and inner height 44.22 ± 0.12 mm was placed under the sieve, which was supported by struts that are disconnected with the vibration machine. Wet grains fell progressively from the sieve into the container once the vibration starts. The free fall height of grains, i.e., the distance between the sieve and the container can be adjusted to control the resulting packing fraction [19]. After the sample preparation, the initial volumetric water content and packing fraction were measured to be $w_0 = 1.7 \pm 0.2\%$ and $\rho_0 = 0.45 \pm 0.01$, respectively.

Drying experiments: The samples were dried at laboratory conditions at temperature of $21 \pm 1 \text{ }^\circ\text{C}$ and 0.55 relative humidity. The weight of each sample was recorded every minute by an analytical balance (Sartorius CP224S) with nominal resolution of 0.1 mg, and photos were taken every 10 minutes by a camera (Canon 600D). Generally, the drying experiment under described conditions took around 45 hours to complete. The end of drying can be identified once the sample weight stops changing and remains at a constant value with fluctuations of the resolution of balance (also indicated by the relatively sharp turning point of drying rate, e.g., in Fig. 2(a)). The completion of drying process was further verified by comparing the residual water content of sample, calculated from the weight difference before and after heating in oven overnight

at 105 °C, to that of dry sample in laboratory condition, both of which were 0.029 ± 0.001%. The cumulative drift of balance was found to be less than 0.5
90 mg during the entire experiment.

MRI profiling experiment: The nuclear magnetic resonance imaging (MRI), as a non-invasive and non-destructive method, has proven effective in probing the evolution of saturation profile during the evaporation process [8, 30, 31]. Here, the drying experiments were also conducted to obtain the
95 evolution of 1D saturation profile using MRI (Bruker Minispec mq20 equipped with a field gradient) under similar experimental conditions as a supplement to provide qualitative characterization of the drying process. Due to the limitation on the size of NMR tube for the mini-spectrometer, the sample size is smaller, i.e, inner diameter of 6.9 mm and inner height of 14.5 mm. Besides, vibration
100 was applied to the container to remove the grains sticking at the inner wall, leading to the initial packing fraction ~0.58 for MRI experiments.

A multi-echo sequence with 128 echos was applied during the evaporation process. The echo time was 7.4 ms, much smaller than the typical relaxation time of the water at 40 ms to avoid a T_2 weighting. The field of view was 20 mm,
105 greater than the sample height. The number of pixels was 128, corresponding to a spatial resolution of 0.16 mm. An averaging by 3 pixels was carried out to smooth the data. The recycle delay was 2 s (much greater than the total duration of the multi-echo sequence and typical value of the longitudinal relaxation time T_1 of the water in this sample) to reach the magnetization equilibrium and
110 to avoid warming of the sample. The signal was accumulated 128 times in order to increase the signal-to-noise ratio, leading to the cycle period of about 4.3 minutes. A Fourier transform of each echo and a Gaussian filter were applied. An exponential fit of odd echos for each pixel was done to get the amplitude, which is proportional to the mass of water corresponding to each pixel. The
115 integration of each 1D profile gives the total NMR signal, which is proportional to the total mass of water.

At the same time, we measured the NMR relaxation through a Carr-Purcell-Meiboom-Gill [32] (CPMG) sequence composed of a first $\pi/2$ -pulse and 2500

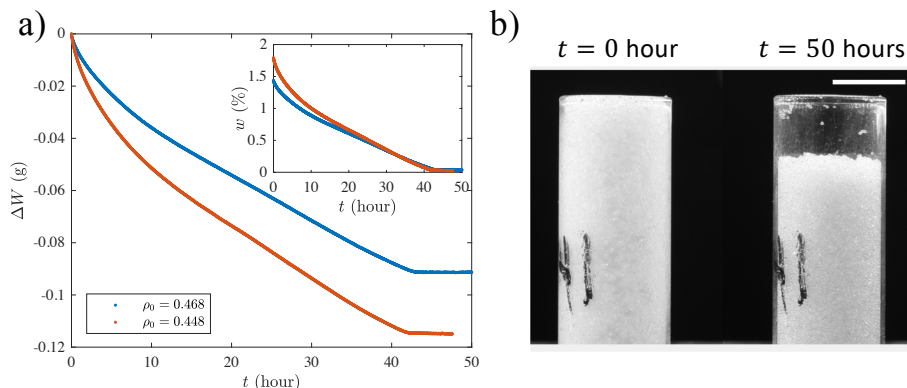


Figure 2: (a) Change of weight as a function of time for two typical experiments with initial packing fractions $\rho_0 = 0.448$ and $\rho_0 = 0.468$. Inset: corresponding water content as a function of time. (b) Photos of sample taken at initial and final stages of drying. Scale bar represents 10 mm.

π -pulses during 500 ms distributed in linear intervals. The repetition time is 2
120 s for relaxation of protons. This sequence was repeated 128 times to increase the signal-to-noise ratio. By means of Inverse Laplace Transform (ILT) with a procedure of non-negative least square fit to the data with Tikhonov regularization (similar to the “Contin” method as in [33, 34]), the transverse relaxation time T_2 distribution can be resolved. We refer to [35] for more details. Note
125 that the 1D profile and CPMG experiments were carried out intermittently in a loop function, leading to an effective time resolution of around 9.9 minutes.

3. Results and Discussion

3.1. Evaporation rate and propagation of drying front

Fig. 2(a) shows the change in sample weight (and water content in the inset)
130 as a function of time for two typical experiments with initial packing fractions of 0.448 and 0.468. For both experiments, the rate of change in weight decreases at the initial stage, entering a roughly linear stage after $t \approx 15$ hours, implying a constant drying period. This is in direct contrast to drying of fully saturated media, where the decreasing rate period occurs after the constant drying regime.

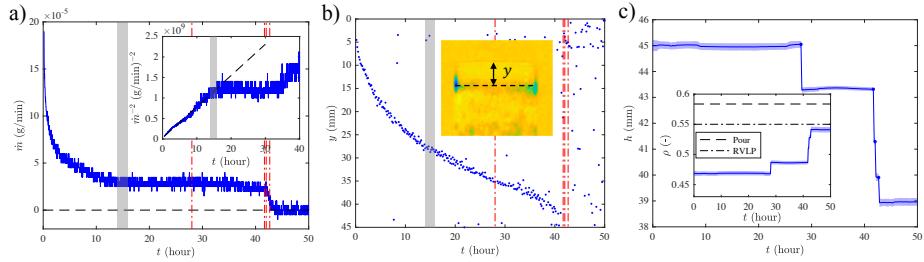


Figure 3: Drying dynamics of a typical experiment. (a) Drying rate \dot{m} as a function of time. Red-dotted lines mark the time of collapse event. Inset: \dot{m}^{-2} as a function of time. Black-dashed line is the linear regression based on data up to $t = 15$ hours. Grey area represents the transition between drying regimes. (b) Depth of drying front versus time. Inset shows the color map of difference between two consecutive images (only top region is shown for visualization purpose). (c) Height of glass beads sample versus time. The identified collapse events are shown as blue dots. Inset: evolution of packing fraction calculated based on sample height. Dashed line and dotted-dashed line represent the packing fractions at dry condition using pouring method (0.58) and random very loose packing (RVLP) state (0.55), respectively. Shaded area represents standard deviation.

135 Fig. 2(b) shows two photos taken at the initial and final stages of drying period, where significant settlement of grains can be seen.

Since the packing fraction is found to be strongly influenced by the interparticle forces [36–43], the drying-induced collapse, as explained earlier, originates from the structural instability of the loosely packed granular material once the liquid bridges evaporate, such that the assembly transitions from cohesive state to cohesionless state as the capillary force diminishes. Although it has been argued that decrease in liquid content does not result in variation in interparticle forces from liquid bridge because the decrease in liquid-solid contact area balances with increase in Laplace pressure [13, 15, 44, 45], at very low liquid content
 140 (asperity or roughness regime [44]), the capillary force decreases sharply with smaller liquid volume due to surface roughness, which has been demonstrated in force measurement experiments in liquid bridges during drying process [46–48]. This implies the existence of a critical water content at which the collapse will be triggered.

150 Fig. 3(a) more clearly shows that the drying rate \dot{m} starts to decrease at the beginning of the experiment, entering a roughly constant rate period after 15 hours (marked by the grey region). Then \dot{m} maintains at this level before decreasing to zero at the end of evaporation. To compare the observed drying rate with evaporation controlled by vapor diffusion, the inset plots \dot{m}^{-2} as a
155 function of time, where a linear relation can be observed during the first 15 hours (black-dashed line), consistent with the theory on the basis of Brutsaert and Chen [1] and experiments during the “second” drying period for initially fully saturated media [9]. This confirms that the liquid bridges can be regarded as effectively isolated, and the effect from film flow is not significant.

160 From image analysis, as shown in Fig. 3(b), the propagation of drying front can be identified through comparing the contrast between two consecutive photos (also see Supporting Information Movie 1). It is found that the speed of receding drying front initially decreases, before entering a constant regime after $t \approx 15$ hours, in line with the transition of drying rate. After the end of drying
165 process (~ 42 hours), the drying front cannot be identified. Fig. 3(c) shows the evolution of sample height h during drying. The changes in h is found to be rather discrete, corresponding to individual collapse events. Also, it can be seen that the majority of the decreases in h occurs near the extreme end of the experiment. The inset shows the corresponding packing fraction determined from
170 images. The times of collapse events are marked as red-dashed-dotted lines in Fig. 3(a) and Fig. 3(b).

To ensure the determination of drying front from image analysis actually reflects the saturation profile within the granular medium, and shed light on the liquid distribution during the drying process, drying experiment was conducted
175 using NMR technique under similar experimental conditions. Fig. 4(a) shows the evolution of 1-D saturation profile during NMR experiment, where light yellow color represents early stage and dark red indicates late times with 50 minutes increments. The saturation, represented by the NMR signal, is found to have similar value along the vertical direction at the start, indicating saturation
180 homogeneity and that the medium is relatively well mixed. As the drying front

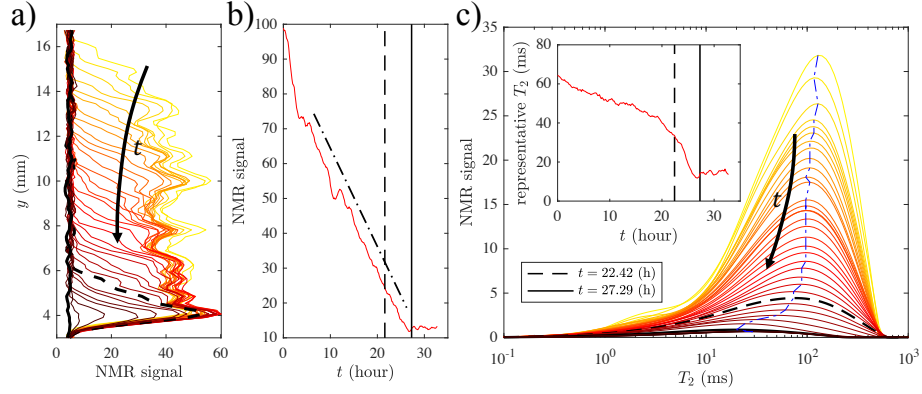


Figure 4: (a) Evolution of the 1-D NMR signal (direct indication of water content) profile. The transition from light yellow to dark red indicates snapshots at progressive time intervals. The time increment for each profile is 50 minutes. (b) Accumulated NMR signal versus time. The black-dashed-dotted line is added only to guide the eye. (c) Evolution of transverse relaxation time T_2 during drying experiment. Blue-dash-dotted line follows the peak value of T_2 at different times. Inset: Evolution of representative T_2 , calculated as the weighted average of the distribution. In all plots, black-dashed lines and black-solid lines denote the same time, i.e., 22.42 hours and 27.29 hours, respectively.

recedes into the medium, the water content remains unchanged below the drying front, whereas the saturation above the drying front drops to a value smaller than the noise of NMR signal (less than $\sim 0.05\%$). Fig. 4(a) also demonstrates that the saturation gradient at the drying front is relatively sharp (around 2
185 mm). It is interesting to note that, visually, the spacing between the 1D profiles is relatively the same, indicating a drying front propagating downwards linearly with time, consistent with the drying regime with relatively constant drying rate. Near the end of drying, a transition can be identified (marked by the black-dashed line). After this transition, the drying region becomes stable in
190 space, and the remaining saturation near the bottom of sample progressively approaches the end state, which is marked by the black-solid line. Fig. 4(b) plots the accumulated NMR signal as a function of time, which is the sum of area under the curve at different times from Fig. 3(a). After an initial sharp drop, the decrease in water content again decreases roughly linearly, consistent

195 with the previous observations. Note that the residual NMR signal after the evaporation finishes was found to be non-zero, which could result from the noise of the NMR signal itself and/or from the irreducible water content (the water content at dry state under laboratory conditions). But this should not influence the result as same signal was found for dry samples.

200 *3.2. Evolution of liquid distribution*

Through CPMG (Carr-Purcell-Meiboom-Gill) experiment [32], the transverse relaxation time T_2 during drying can be obtained, which reads as [49, 50]:

$$\frac{1}{T_2} \approx \lambda \frac{S}{V} + \frac{1}{T_2^{\text{bulk}}} \approx \lambda \frac{S}{V}, \quad (1)$$

where λ is the surface relaxivity (unit: m/s), T_2^{bulk} is the relaxation time of bulk water, S is the wet surface area, and V is the volume of water. The term from T_2^{bulk} can be neglected in Eqn. (1) according to Tarr and Brownstein criterion [51] since the dimensionless parameter $a\lambda/D$ is found to be much less than 1, corresponding to the fast diffusion region (also denoted as surface limited relaxation), where a is the characteristic size of liquid cluster, and $D \approx 2.3 \times 10^{-9} \text{ m}^2\text{s}^{-1}$ is water self-diffusion coefficient at 25 °C [52]. Fig. 4(c) shows the evolution of T_2 distributions, where the arrow indicates increasing time. At early times, a peak at $T_2 \approx 100$ ms can be seen. If look closely, a secondary peak is also present at $T_2 \approx 2$ ms. Since liquid in non-saturated granular material can exist in the form of both liquid bridges between grains and thin films on grain surface [10, 12, 26, 53], it is likely that populations in the vicinities of $T_2 \approx 100$ ms and $T_2 \approx 2$ ms correspond to the liquid bridges and thin films, respectively. To test this hypothesis, for given initial volumetric water content, assuming liquid bridges contribute to the majority of liquid volume, we can estimate the average volume of liquid bridge in monodisperse spheres assuming a coordination number $N \approx 6$ [54, 55]. Then, using the relation [56]:

$$V = 0.12d_p^3 \sin^4(\beta)C_aC_\theta, \quad (2)$$

220 the half-filling angle β can be obtained, where d_p is particle diameter, $C_a = 1$ for particles in contact, and $C_\theta = 1 + 1.1 \sin \theta$ is the correction factor for contact

angle θ . Finally, the volume-to-area ratio can be expressed as:

$$\frac{V}{S} = \frac{0.12d_p^3 \sin^4(\beta) C_a C_\theta}{\pi(1 - \cos \beta)}. \quad (3)$$

From Eqn. (3) and Eqn. (1), combined with the ratio of T_2 of two populations, the average thickness of thin film, which is simply calculated as $h = V/S$, is found to be $h \in [0.17, 0.25] \mu\text{m}$ for contact angle $\theta \in [0^\circ, 60^\circ]$. Past studies have indicated that the film thickness h is of the same order as roughness of grains [57]. For example, the film thickness is found to be $h \sim 0.6 \mu\text{m}$ for Fontainebleau sandstone of roughness depth $1 \mu\text{m}$ [57]. Thus, for typical glass beads of roughness $\sim 0.5 \mu\text{m}$ [10], the film thickness is expected to be $\sim 0.3 \mu\text{m}$, which agrees well with the calculated value. To check the assumption that the total volume of liquid film is much smaller than that of liquid bridges, the volumetric water content under the condition where all surface areas are covered by thin film is found to be $\sim 0.2\%$, much smaller than the total initial water content of $\sim 4.3\%$ in NMR experiment.

Therefore, Fig. 4(c) implies that the liquid exist mainly in the form of liquid bridges (high NMR signal), and the contribution from the thin films can be effectively ignored. The trajectory of T_2 with maximum NMR signal is shown as blue-dot-dashed line. It remains almost constant before the transition marked by black-dashed line, then experiencing a sharp decrease. This is indeed consistent with the previous observation where the drying front recedes into the porous medium, leading to a significant decrease in total volume of liquid (corresponding to decrease in NMR signal), but with no significant change of the geometrical feature of liquid clusters (corresponding to constant T_2). The latter is mainly represented by the volume-to-area ratio of the liquid bridges that make up the bulk of liquid volumes (those below the drying front). The volume-to-area ratio only starts to decrease near the end of drying, corresponding to a drying region that is stable in space (Fig. 4(a) after the black-dashed line), during which the representative volume of liquid bridges decreases. Similar tendency can be reflected from the representative T_2 (Inset of Fig. 4(c)), calculated as the weighted average of T_2 distribution at different times, where it decreases

slowly before $t = 22.4$ h due to the weighted averaging process, and a sharp decrease can be observed after the transition. It is interesting to note that the spatial shift of saturation profile (front propagation) in Fig. 4(a) corresponds to the decrease in signal intensity of T_2 distribution in Fig. 4(c), whereas a spatially stable decrease in saturation after the transition ($t = 22.4$ h) corresponds to the shift in value of representative T_2 . These observations together reveal the global and local evolution of volume and shape of liquid clusters.

3.3. *Drying-induced collapse*

Given the observation of the drying front and sharp saturation gradient propagating downwards continuously, one would expect similar statistics of collapse events that are correlated with the drying front. However, surprisingly, Fig. 3(c) shows that the collapse events (blue dots) occur in a rather discrete manner, with most collapse events occurring at the very end of drying. This has two implications. Firstly, liquid bridges exist in the dry region above the drying front with corresponding water content that is too small to be detected by NMR technique (less than $\sim 0.05\%$), but sufficient to support the loose structure of the medium. Although we are unable to find past works on the critical liquid content that marks the onset of most drying-induced collapses, the variations of the tensile/shear strength of non-saturated granular materials, as well as the packing fraction of wet grains, should bear the indicative information on the critical liquid content, as the fundamental grain-scale mechanism that controls the aforementioned macroscopic behaviours is the interparticle cohesive forces due to liquid bridges. For spherical grains such as glass beads, the threshold liquid content is indeed found to be rather small ($< 1\%$) [12, 16, 58]. Particularly, the degree of saturation at maximum shear-wave velocity, which is directly related to the shear modulus, is determined to be $\sim 0.7\%$ [58], below which the shear modulus plummets with decreasing water content. This critical liquid content can be effectively regarded as an upper bound for the critical saturation for the collapse, since the unstable loosely-packed structure will not be able to withstand gravity of particles once the enhancement in interparticle frictional

resistance due to liquid bridges (reflected by shear modulus) is reduced. Note that this threshold value is likely to be sensitive to particle shapes and grain size distribution [58–61], which is worth investigating in future works.

Secondly, contrary to past hypothesis that the liquid in the apparent dry
285 region cannot be further extracted and equals to the air-dry value [8, 62], it indeed can be further reduced near the end of drying, which is signaled by the collapse events.

To ensure the repeatability of the experiments and gain sufficient statistical information on drying-induced collapse, the sample height versus time from six
290 experiments are plotted in Fig. 5(a). Again, concentrated collapses are observed at $t \approx 40$ hours depending on initial water content and minor fluctuations in relative humidity and temperature, and almost no collapse event occurs in the first 30 hours even with significant apparent dry region after propagation of drying front (Fig. 3(c)). The corresponding packing fraction ρ calculated from
295 image analysis is shown in Fig. 5(b). The solid and dot-dashed lines represent the packing fractions measured at dry condition using pouring method [19] and lower limit of random very loose packing (RVLP) [20–23], respectively. As can be seen in Fig. 5(b), the packing fraction increases from ~ 0.45 to ~ 0.55 after collapse, close to the RVLP. Note that there is an underestimation of the packing
300 fraction, as the surface is no longer perfectly smooth after collapse such that the occupied volumes of particles determined from 2D images are typically greater than actual ones. This may explain some of the final packing fractions are still smaller than the RVLP limit.

Apart from the identification of drying front and collapse height, the indi-
305 vidual collapse region, characterized by its length l_c can also be obtained from the image analysis. Fig. 5(c) shows the image contrast (subtraction of image matrix) before ($c_n - 1$), at (c_n), and after ($c_n + 1$) an individual collapse event. Three distinct regions can be identified: (1) large contrast region with cumulative horizontal contrast above 2000, which represents the region that is filled
310 before the collapse, but empty after; (2) moderate contrast region with contrast smaller than 2000 and greater than 300, which represents the region that

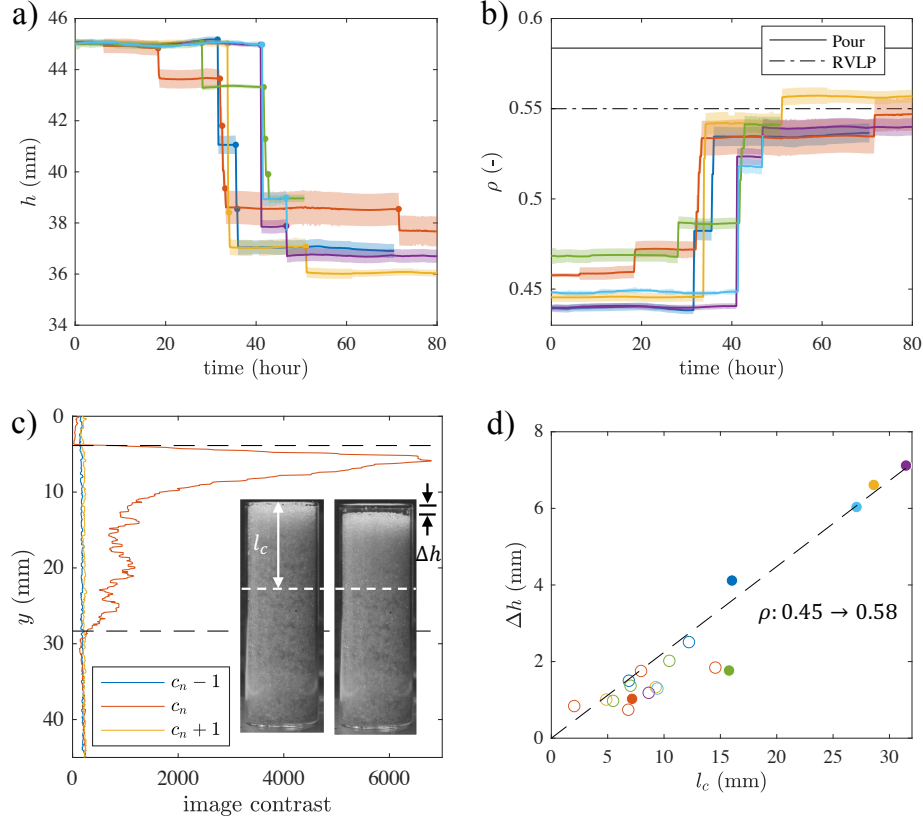


Figure 5: (a) Height versus time for six repeated experiments. Concentrated collapse events are observed near the end of drying ($t \approx 40$ hours). (b) Corresponding packing fraction determined from the image analysis. Solid line and dotted-dashed line represent the packing fractions at dry condition using pouring method (0.58) and random very loose packing (RVLVP) state (0.55), respectively. (c) Typical data of the sum in the horizontal direction of difference of two consecutive images right before ($c_n - 1$), at (c_n), and right after ($c_n + 1$) a collapse event. Distance between the black-dashed lines represents the individual collapse region length l_c . Inset: photos right before/after a collapse event. The region above the white-dashed line collapses, whereas the region below remains unaffected. (d) Statistics of collapse events for six experiments: change in height Δh versus individual collapse region length l_c . Filled and hollow symbols represent the first and subsequent collapse events, respectively. Black-dashed line shows the theory when packing fraction changes from 0.45 to 0.58 homogeneously.

is filled with initial packing state, but collapses into different (denser) packing state after; (3) small contrast region with contrast less than 300, where there is no change in structure and the fluctuations are mainly from image noise.

315 Note that the changes in image contrast at the boundaries of different regions are relatively sharp, and it is found that minor variations in these empirically selected threshold values do not significantly impact the results. In the case of Fig. 5(c), the distance between the black-dashed lines is thus l_c . Note that the individual collapse region length l_c is calculated as the effective one, i.e, it

320 only represents the region that evolves from loose state towards denser state at each individual collapse, without the cumulative effect from previous collapses. The inset shows the photos before and after an initial collapse event, where the region below the white-dashed line remain unaffected. This suggests that even in the apparent dry region, there exists a saturation gradient, which may

325 correspond to a *third* drying front that separates the sample by the effectiveness of the capillary bridge through a critical water content. The region below this drying front can withstand the impact of collapse above it and remain intact due to the capillary force. As one of the main findings, this *third* drying front has not been discovered before. However, a more thorough investigation requires higher resolution of measuring device and more controlled experimental

330 condition, which is beyond the scope of current work.

Fig. 5(d) depicts the correlation between change in height and individual collapse region length. Filled and hollow circles represent initial and subsequent collapse events for each experiment in different colors. It shows that the initial

335 collapse events tend to have greater region of impact. In addition, most points can be described by a theoretical line assuming the packing fraction changes from 0.45 to 0.58 for each individual collapse event. This again indicates that the nature of collapse is local. Besides, it shows that both the initial packing structure before collapse, and the change in packing fraction for each individual

340 collapse event, are relatively homogeneous.

3.4. Transition in drying regimes

One possible reason that results in the observed transition in drying regimes could be the theory of enhanced vapour diffusion in non-saturated porous media [63, 64], i.e., in the presence of thermal or capillary gradient, the vapor can
345 condensate on one side of liquid island and subsequently evaporate from the other side, which reduces the effective diffusion path length. Nevertheless, the enhancement factor in this model decreases with decreasing saturation, being close to one at low saturation [64]. Since the initial water content is also low in the current study ($\sim 2\%$), and the transition takes place in later stage of
350 drying (at even lower water content), the enhanced diffusion theory alone cannot explain the observed results.

Besides, the effect from film flow at low water content regime has been explored in the recent years [25–28, 53, 62], where the liquid connectivity is maintained through the thin liquid film at the grain surface. As a result, the
355 drying flux through the film flow is proportional to the specific surface area of the granular medium, which implies that the drying flux at transition in drying regimes, if mainly transported through film flow, should be sensitive to the grain size. However, we did not observe this phenomenon and the critical drying rate at which the transition occurs is similar for $376 \pm 32 \mu\text{m}$ and $1594 \pm 171 \mu\text{m}$
360 glass beads (Fig. A.1 in the Appendix).

Actually, it is likely that the observed phenomena is due to Kelvin effect. The Kelvin equation $\ln p^* = \gamma V_m / rRT$ indicates that the relative vapor pressure at the liquid-gas interface p^* depends on the capillary pressure γ/r , with γ surface tension, r the radius of curvature of liquid-gas interface, R universal gas
365 constant, and T temperature. As the drying front propagates and the region of the porous medium above it approaches dry condition, the curvature of liquid bridges quickly increases, leading to drop in vapor pressure at the surface of liquid bridges, slowing down the drying process of those very small liquid bridges in the apparent dry region, which explains the existence of liquid in the apparent
370 dry region. As the evaporation proceeds, the overall drying rate decreases due to greater diffusion distance according to Fick's law, whereas a greater number of

menisci are exposed to evaporation, thus leading to a deviation from the theory where Kelvin effect (and thus the presence of liquids above the drying front) is not considered. The enhancement in drying rate due to Kelvin effect is also
375 reported in a recent work using pore-network simulation [65]. It is worth noting that this phenomenon can be regarded as an equilibration process [8]. However, different from capillary flow where the equilibration takes place within liquid phase due to difference in capillary pressure, it is due to constrain in the vapor pressure according to Kelvin equation. Although without detailed discussion,
380 similar drying enhancement phenomenon at low saturation (less than 5%) is also present in the study by Thiery et al [8]. In fact, the Kelvin effect can be significant either for very fine particles or very low water content [8, 66], and the current study demonstrates for the first time the drying enhancement phenomenon due to Kelvin effect for grains with size of hundreds of micrometers.

385 **4. Conclusions**

The drying of loosely packed granular materials from low initial water content was experimentally studied. The drying rate is found to decrease from the beginning, corresponding to the decreasing rate period controlled by vapor diffusion, which is associated with a propagation of drying front with a sharp
390 saturation gradient identified through image analysis and magnetic resonance imaging. Then, a deviation in drying rate from diffusion limited evaporation is observed. The enhancement of the evaporation at the later stage of drying process is attributed to Kelvin effect.

We also observed the drying-induced collapse of granular medium due to
395 its structural instability as the liquid bridges evaporate and capillary forces decrease. The concentrated collapse at the end of drying suggests the existence of liquid in the form of liquid bridges in the apparent dry region due to Kelvin effect, which can be further extracted near the end of drying process. Through analyzing the collapse statistics, it is found that collapse event is local in space
400 and time, which implies that, apart from previously identified primary and

secondary drying fronts, there exists a *third* drying front in the apparent dry region, which propagates relatively quickly at the end of drying.

Acknowledgments

This work was financially supported by Australian Research Council (Projects
405 DP170102886) and The University of Sydney SOAR Fellowship. YG acknowl-
edges the financial support of Labex MMCD(ANR-11-LABX-022-01) for his stay
at Laboratoire Navier at ENPC. ZW thanks Baptiste Chabot, Xavier Boulay,
Loïc Lesueur, and Emmanuel De Laure for the assistance on experiments. Data
associated with this work are available online ([https://doi.org/10.6084/m9.
410 figshare.14368688](https://doi.org/10.6084/m9.figshare.14368688)).

Appendix

Fig. A.1 shows the drying curves (evolution of sample weight, drying rate \dot{m} ,
and \dot{m}^{-2}) for grains at different initial packing fractions (a-c) and larger grain
size (d). The black-solid lines are linear fittings based on data at early stages of
415 drying, which represent the theory predicted based on Fick's law. An enhance-
ment in drying rate can be observed in all experiments, which corresponds to
a downward deviation from the linear relation. The drying rates at which this
transition occurs are ~ 3 g/min for all cases (as in \dot{m} - t plots).

References

- 420 [1] W. Brutsaert, D. Chen, Desorption and the two stages of drying
of natural tallgrass prairie, Water Resources Research 31 (5) (1995)
1305–1313. arXiv:[https://agupubs.onlinelibrary.wiley.com/doi/
pdf/10.1029/95WR00323](https://agupubs.onlinelibrary.wiley.com/doi/pdf/10.1029/95WR00323), doi:<https://doi.org/10.1029/95WR00323>.
URL [https://agupubs.onlinelibrary.wiley.com/doi/abs/10.1029/
425 95WR00323](https://agupubs.onlinelibrary.wiley.com/doi/abs/10.1029/95WR00323)

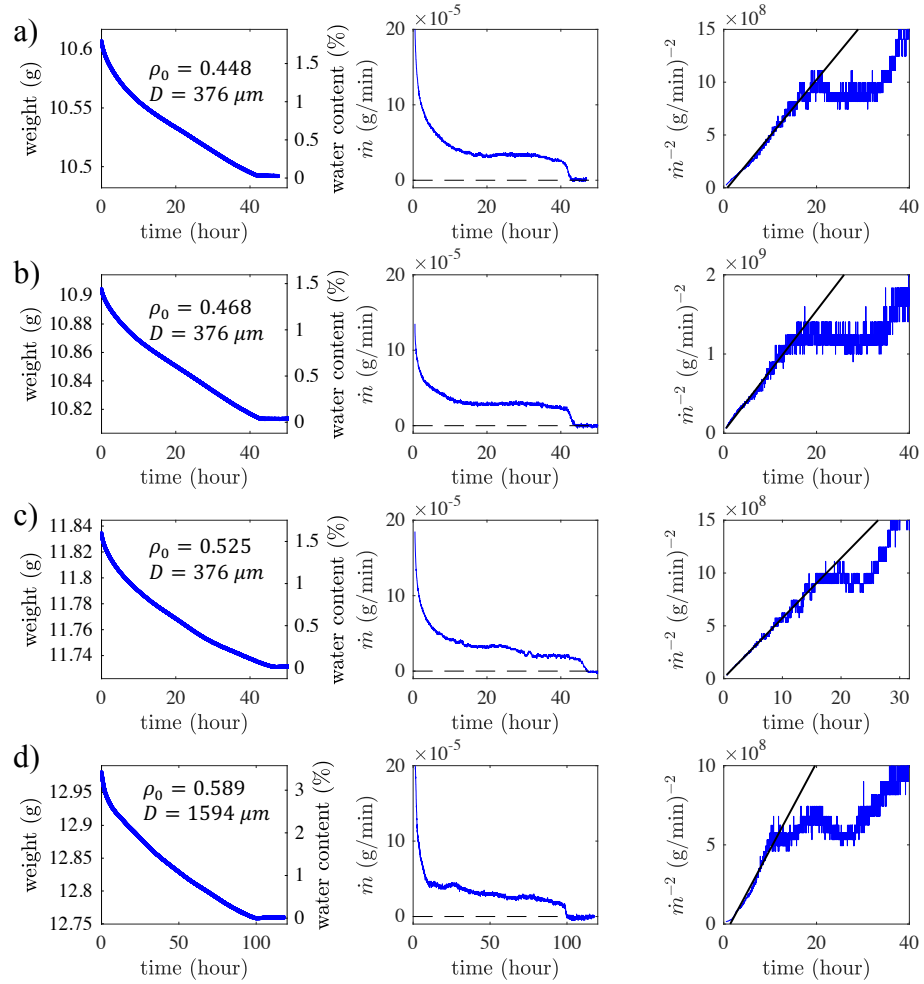


Figure A.1: Drying curves of unsaturated porous media. (a-c) Glass beads of diameter 375.5 ± 31.8 and different initial packing fractions. (d) Glass beads of diameter 1594 ± 171 . Solid lines are linear fittings using data at the early stages.

- [2] P. Coussot, Scaling approach of the convective drying of a porous medium, *The European Physical Journal B - Condensed Matter and Complex Systems* 15 (3) (2000) 557–566. doi:10.1007/s100510051160.
URL <https://doi.org/10.1007/s100510051160>
- 430 [3] D. Or, P. Lehmann, E. Shakraeni, N. Shokri, Advances in Soil Evaporation Physics—A Review, *Vadose Zone Journal* 12 (4), vzj2012.0163. arXiv:<https://pubs.geoscienceworld.org/vzj/article-pdf/12/4/vzj2012.0163/2983949/vzj2012.0163.pdf>, doi:10.2136/vzj2012.0163.
435 URL <https://doi.org/10.2136/vzj2012.0163>
- [4] N. Shokri, P. Lehmann, D. Or, Critical evaluation of enhancement factors for vapor transport through unsaturated porous media, *Water Resources Research* 45 (10). arXiv:<https://agupubs.onlinelibrary.wiley.com/doi/pdf/10.1029/2009WR007769>, doi:<https://doi.org/10.1029/2009WR007769>.
440 URL <https://agupubs.onlinelibrary.wiley.com/doi/abs/10.1029/2009WR007769>
- [5] P. Lehmann, S. Assouline, D. Or, Characteristic lengths affecting evaporative drying of porous media, *Phys. Rev. E* 77 (2008) 056309. doi:10.1103/PhysRevE.77.056309.
445 URL <https://link.aps.org/doi/10.1103/PhysRevE.77.056309>
- [6] A. G. Yiotis, D. Salin, E. S. Tajer, Y. C. Yortsos, Analytical solutions of drying in porous media for gravity-stabilized fronts, *Phys. Rev. E* 85 (2012) 046308. doi:10.1103/PhysRevE.85.046308.
450 URL <https://link.aps.org/doi/10.1103/PhysRevE.85.046308>
- [7] A. G. Yiotis, D. Salin, E. S. Tajer, Y. C. Yortsos, Drying in porous media with gravity-stabilized fronts: Experimental results, *Phys. Rev. E* 86 (2012) 026310. doi:10.1103/PhysRevE.86.026310.
URL <https://link.aps.org/doi/10.1103/PhysRevE.86.026310>

- 455 [8] J. Thiery, S. Rodts, D. A. Weitz, P. Coussot, Drying regimes in homogeneous porous media from macro- to nanoscale, *Phys. Rev. Fluids* 2 (2017) 074201. doi:10.1103/PhysRevFluids.2.074201.
URL <https://link.aps.org/doi/10.1103/PhysRevFluids.2.074201>
- [9] N. Shokri, D. Or, What determines drying rates at the onset of diffusion controlled stage-2 evaporation from porous media?, *Water Resources Research* 47 (9). arXiv:<https://agupubs.onlinelibrary.wiley.com/doi/pdf/10.1029/2010WR010284>, doi:<https://doi.org/10.1029/2010WR010284>.
URL <https://agupubs.onlinelibrary.wiley.com/doi/abs/10.1029/2010WR010284>
- 460 [10] Z. Fournier, D. Geromichalos, S. Herminghaus, M. M. Kohonen, F. Mugele, M. Scheel, M. Schulz, B. Schulz, C. Schier, R. Seemann, A. Skudelný, Mechanical properties of wet granular materials, *Journal of Physics: Condensed Matter* 17 (9) (2005) S477–S502.
- 470 [11] V.-D. Than, P. Aïmediou, J.-M. Pereira, J.-N. Roux, M. Bornert, A.-M. Tang, Macro-microscopic one-dimensional compression of wet granular soils by experimental investigation, *E3S Web of Conferences* 9 (2016) 06001.
- [12] M. Scheel, R. Seemann, M. Brinkmann, M. Di Michiel, A. Sheppard, B. Breidenbach, S. Herminghaus, Morphological clues to wet granular pile stability, *Nature materials* 7 (2008) 189–93.
- 475 [13] Y. I. Rabinovich, M. S. Esayanur, B. M. Moudgil, Capillary forces between two spheres with a fixed volume liquid bridge: Theory and experiment, *Langmuir* 21 (24) (2005) 10992–10997, pMID: 16285763.
- [14] M. Scheel, R. Seemann, M. Brinkmann, M. D. Michiel, A. Sheppard, S. Herminghaus, Liquid distribution and cohesion in wet granular assemblies beyond the capillary bridge regime, *Journal of Physics: Condensed Matter* 20 (49) (2008) 494236.
- 480

- [15] H.-J. Butt, M. Kappl, Normal capillary forces, *Advances in Colloid and Interface Science* 146 (1) (2009) 48 – 60.
- 485 [16] C. Feng, A. Yu, Effect of liquid addition on the packing of mono-sized coarse spheres, *Powder Technology* 99 (1) (1998) 22 – 28.
- [17] R. Y. Yang, R. P. Zou, A. B. Yu, Numerical study of the packing of wet coarse uniform spheres, *AIChE Journal* 49 (7) (2003) 1656–1666.
- [18] N. Mitarai, F. Nori, Wet granular materials, *Advances in Physics* 55 (1-2)
490 (2006) 1–45.
- [19] Z. Wang, J.-M. Pereira, Y. Gan, Packing of wet monodisperse spheres, *Powder Technology* 378 (2021) 60 – 64. doi:<https://doi.org/10.1016/j.powtec.2020.09.074>.
URL <http://www.sciencedirect.com/science/article/pii/S0032591020309384>
495
- [20] G. Y. Onoda, E. G. Liniger, Random loose packings of uniform spheres and the dilatancy onset, *Phys. Rev. Lett.* 64 (1990) 2727–2730.
- [21] M. P. Ciamarra, A. Coniglio, Random very loose packings, *Phys. Rev. Lett.* 101 (2008) 128001.
- 500 [22] M. Jerkins, M. Schröter, H. L. Swinney, T. J. Senden, M. Saadatfar, T. Aste, Onset of mechanical stability in random packings of frictional spheres, *Phys. Rev. Lett.* 101 (2008) 018301.
- [23] G. R. Farrell, K. M. Martini, N. Menon, Loose packings of frictional spheres, *Soft Matter* 6 (2010) 2925–2930.
- 505 [24] T. T. Vo, S. Nezamabadi, P. Mutabaruka, J.-Y. Delenne, F. Radjai, Additive rheology of complex granular flows, *Nature Communications* 11 (1) (2020) 1476. doi:[10.1038/s41467-020-15263-3](https://doi.org/10.1038/s41467-020-15263-3).
URL <https://doi.org/10.1038/s41467-020-15263-3>

- [25] M. Tuller, D. Or, Hydraulic conductivity of variably saturated porous media: Film and corner flow in angular pore space, *Water Resources Research* 37 (5) (2001) 1257–1276. arXiv:<https://agupubs.onlinelibrary.wiley.com/doi/pdf/10.1029/2000WR900328>, doi:<https://doi.org/10.1029/2000WR900328>.
URL <https://agupubs.onlinelibrary.wiley.com/doi/abs/10.1029/2000WR900328>
- [26] M. Tuller, D. Or, Water films and scaling of soil characteristic curves at low water contents, *Water Resources Research* 41 (9). arXiv:<https://agupubs.onlinelibrary.wiley.com/doi/pdf/10.1029/2005WR004142>, doi:<https://doi.org/10.1029/2005WR004142>.
URL <https://agupubs.onlinelibrary.wiley.com/doi/abs/10.1029/2005WR004142>
- [27] Y. Wang, J. Ma, Y. Zhang, M. Zhao, W. M. Edmunds, A new theoretical model accounting for film flow in unsaturated porous media, *Water Resources Research* 49 (8) (2013) 5021–5028. arXiv:<https://agupubs.onlinelibrary.wiley.com/doi/pdf/10.1002/wrcr.20390>, doi:<https://doi.org/10.1002/wrcr.20390>.
URL <https://agupubs.onlinelibrary.wiley.com/doi/abs/10.1002/wrcr.20390>
- [28] Y. Wang, M. Jin, Z. Deng, Alternative model for predicting soil hydraulic conductivity over the complete moisture range, *Water Resources Research* 54 (9) (2018) 6860–6876. arXiv:<https://agupubs.onlinelibrary.wiley.com/doi/pdf/10.1029/2018WR023037>, doi:<https://doi.org/10.1029/2018WR023037>.
URL <https://agupubs.onlinelibrary.wiley.com/doi/abs/10.1029/2018WR023037>
- [29] J.-F. Bruchon, J.-M. Pereira, M. Vandamme, N. Lenoir, P. Delage, M. Bornert, Full 3d investigation and characterisation of capillary collapse

- of a loose unsaturated sand using x-ray ct, *Granular Matter* 15 (6) (2013) 783–800. doi:10.1007/s10035-013-0452-6.
- 540 URL <https://doi.org/10.1007/s10035-013-0452-6>
- [30] N. Ben Abdelouahab, A. Gossard, S. Rodts, B. Coasne, P. Coussot, Convective drying of a porous medium with a paste cover, *The European Physical Journal E* 42 (5) (2019) 66. doi:10.1140/epje/i2019-11829-4.
- URL <https://doi.org/10.1140/epje/i2019-11829-4>
- 545 [31] P. Coussot, Progress in rheology and hydrodynamics allowed by nmr or mri techniques, *Experiments in Fluids* 61 (9) (2020) 207. doi:10.1007/s00348-020-03037-y.
- URL <https://doi.org/10.1007/s00348-020-03037-y>
- [32] S. Meiboom, D. Gill, Modified Spin-Echo Method for Measuring Nuclear Relaxation Times, *Review of Scientific Instruments* 29 (8) (1958) 688–691.
- 550 doi:10.1063/1.1716296.
- [33] S. W. Provencher, A constrained regularization method for inverting data represented by linear algebraic or integral equations, *Computer Physics Communications* 27 (3) (1982) 213 – 227.
- 555 doi:[https://doi.org/10.1016/0010-4655\(82\)90173-4](https://doi.org/10.1016/0010-4655(82)90173-4).
- URL <http://www.sciencedirect.com/science/article/pii/0010465582901734>
- [34] K. P. Whittall, A. L. MacKay, Quantitative interpretation of nmr relaxation data, *Journal of Magnetic Resonance* (1969) 84 (1) (1989) 134 – 152.
- 560 doi:[https://doi.org/10.1016/0022-2364\(89\)90011-5](https://doi.org/10.1016/0022-2364(89)90011-5).
- URL <http://www.sciencedirect.com/science/article/pii/0022236489900115>
- [35] P. F. Faure, S. Rodts, Proton nmr relaxation as a probe for setting cement pastes, *Magnetic Resonance Imaging* 26 (8) (2008) 1183 – 1196.
- 565 doi:<https://doi.org/10.1016/j.mri.2008.01.026>.

URL <http://www.sciencedirect.com/science/article/pii/S0730725X08000520>

- [36] R. Y. Yang, R. P. Zou, A. B. Yu, Computer simulation of the packing of fine particles, *Phys. Rev. E* 62 (2000) 3900–3908.
- 570 [37] A. Yu, C. Feng, R. Zou, R. Yang, On the relationship between porosity and interparticle forces, *Powder Technology* 130 (1) (2003) 70 – 76.
- [38] J. Blum, R. Schräpler, Structure and mechanical properties of high-porosity macroscopic agglomerates formed by random ballistic deposition, *Phys. Rev. Lett.* 93 (2004) 115503.
- 575 [39] D. Lohse, R. Rauhé, R. Bergmann, D. Meer, Creating a dry variety of quicksand, *Nature* 432 (2005) 689–90.
- [40] K. J. Dong, R. Y. Yang, R. P. Zou, A. B. Yu, Role of interparticle forces in the formation of random loose packing, *Phys. Rev. Lett.* 96 (2006) 145505.
- [41] P. B. Umbanhowar, D. I. Goldman, Low density fragile states in cohesive powders, *American Journal of Physics* 74 (8) (2006) 720–721.
- 580 [42] R. Yang, R. Zou, K. Dong, X. An, A. Yu, Simulation of the packing of cohesive particles, *Computer Physics Communications* 177 (1) (2007) 206 – 209, proceedings of the Conference on Computational Physics 2006.
- [43] E. Parteli, J. Schmidt, C. Blümel, K.-E. Wirth, W. Peukert, T. Pöschel, Attractive particle interaction forces and packing density of fine glass powders, *Scientific reports* 4 (2014) 6227.
- 585 [44] T. C. Halsey, A. J. Levine, How sandcastles fall, *Phys. Rev. Lett.* 80 (1998) 3141–3144.
- [45] H.-J. Butt, Capillary forces: Influence of roughness and heterogeneity, *Langmuir* 24 (9) (2008) 4715–4721, PMID: 18442225.
- 590

- [46] B. Mielniczuk, T. Hueckel, M. S. E. Youssefi, Evaporation-induced evolution of the capillary force between two grains, *Granular Matter* 16 (5) (2014) 815–828. doi:[10.1007/s10035-014-0512-6](https://doi.org/10.1007/s10035-014-0512-6).
URL <https://doi.org/10.1007/s10035-014-0512-6>
- 595 [47] B. Mielniczuk, T. Hueckel, M. S. El Youssefi, Laplace pressure evolution and four instabilities in evaporating two-grain liquid bridges, *Powder Technology* 283 (2015) 137 – 151. doi:<https://doi.org/10.1016/j.powtec.2015.05.024>.
URL <http://www.sciencedirect.com/science/article/pii/S0032591015004106>
- 600 [48] T. Hueckel, B. Mielniczuk, M. S. El Youssefi, Adhesion-force micro-scale study of desiccating granular material, *Géotechnique* 70 (12) (2020) 1133–1144. arXiv:<https://doi.org/10.1680/jgeot.18.P.298>, doi:[10.1680/jgeot.18.P.298](https://doi.org/10.1680/jgeot.18.P.298).
605 URL <https://doi.org/10.1680/jgeot.18.P.298>
- [49] R. M. E. Valckenborg, L. Pel, K. Hazrati, K. Kopinga, J. Marchand, Pore water distribution in mortar during drying as determined by nmr, *Materials and Structures* 34 (10) (2001) 599–604. doi:[10.1007/BF02482126](https://doi.org/10.1007/BF02482126).
URL <https://doi.org/10.1007/BF02482126>
- 610 [50] A. Valori, P. McDonald, K. Scrivener, The morphology of c–s–h: Lessons from 1h nuclear magnetic resonance relaxometry, *Cement and Concrete Research* 49 (2013) 65 – 81. doi:<https://doi.org/10.1016/j.cemconres.2013.03.011>.
URL <http://www.sciencedirect.com/science/article/pii/S0008884613000653>
- 615 [51] K. R. Brownstein, C. E. Tarr, Importance of classical diffusion in nmr studies of water in biological cells, *Phys. Rev. A* 19 (1979) 2446–2453. doi:[10.1103/PhysRevA.19.2446](https://doi.org/10.1103/PhysRevA.19.2446).
URL <https://link.aps.org/doi/10.1103/PhysRevA.19.2446>

- 620 [52] M. Holz, S. R. Heil, A. Sacco, Temperature-dependent self-diffusion coefficients of water and six selected molecular liquids for calibration in accurate 1h nmr pfg measurements, *Phys. Chem. Chem. Phys.* 2 (2000) 4740–4742. doi:10.1039/B005319H.
URL <http://dx.doi.org/10.1039/B005319H>
- 625 [53] Y. Wang, J. Ma, H. Guan, A mathematically continuous model for describing the hydraulic properties of unsaturated porous media over the entire range of matric suctions, *Journal of Hydrology* 541 (2016) 873 – 888. doi:<https://doi.org/10.1016/j.jhydro.2016.07.046>.
URL <http://www.sciencedirect.com/science/article/pii/S0022169416304760>
- 630 [54] L. Liu, Z. Zhang, A. Yu, Dynamic simulation of the centripetal packing of mono-sized spheres, *Physica A: Statistical Mechanics and its Applications* 268 (3) (1999) 433 – 453.
- [55] W. Fei, G. A. Narsilio, Impact of three-dimensional sphericity and roundness on coordination number, *Journal of Geotechnical and Geoenvironmental Engineering* 146 (12) (2020) 06020025.
- 635 [56] T. Weigert, S. Ripperger, Calculation of the liquid bridge volume and bulk saturation from the half-filling angle, *Particle & Particle Systems Characterization* 16 (5) (1999) 238–242.
- [57] M. Han, S. Youssef, E. Rosenberg, M. Fleury, P. Levitz, Deviation from archie’s law in partially saturated porous media: Wetting film versus disconnectedness of the conducting phase, *Phys. Rev. E* 79 (2009) 031127. doi:10.1103/PhysRevE.79.031127.
URL <https://link.aps.org/doi/10.1103/PhysRevE.79.031127>
- 640 [58] G. C. Cho, J. C. Santamarina, Unsaturated particulate materials—particle-level studies, *Journal of Geotechnical and Geoenvironmental Engineering* 127 (1) (2001) 84–96. doi:10.1061/(ASCE)1090-0241(2001)127:1(84).

- [59] S. Wu, D. H. Gray, F. E. Richart, Capillary effects on dynamic modulus of
650 sands and silts, *Journal of Geotechnical Engineering* 110 (9) (1984) 1188–
1203. doi:10.1061/(ASCE)0733-9410(1984)110:9(1188).
- [60] R.-P. Zou, C.-L. Feng, A.-B. Yu, Packing density of binary mix-
tures of wet spheres, *Journal of the American Ceramic Society*
84 (3) (2001) 504–508. arXiv:[https://ceramics.onlinelibrary.wiley.
655 com/doi/pdf/10.1111/j.1151-2916.2001.tb00690.x](https://ceramics.onlinelibrary.wiley.com/doi/pdf/10.1111/j.1151-2916.2001.tb00690.x), doi:10.1111/j.
1151-2916.2001.tb00690.x.
URL [https://ceramics.onlinelibrary.wiley.com/doi/abs/10.1111/
j.1151-2916.2001.tb00690.x](https://ceramics.onlinelibrary.wiley.com/doi/abs/10.1111/j.1151-2916.2001.tb00690.x)
- [61] R. Zou, J. Xu, C. Feng, A. Yu, S. Johnston, N. Standish, Packing of multi-
660 sized mixtures of wet coarse spheres, *Powder Technology* 130 (1) (2003)
77 – 83. doi:[https://doi.org/10.1016/S0032-5910\(02\)00229-2](https://doi.org/10.1016/S0032-5910(02)00229-2).
URL [http://www.sciencedirect.com/science/article/pii/
S0032591002002292](http://www.sciencedirect.com/science/article/pii/S0032591002002292)
- [62] Y. Wang, O. Merlin, G. Zhu, K. Zhang, A physically based method
665 for soil evaporation estimation by revisiting the soil drying process,
Water Resources Research 55 (11) (2019) 9092–9110. arXiv:[https://
agupubs.onlinelibrary.wiley.com/doi/pdf/10.1029/2019WR025003](https://agupubs.onlinelibrary.wiley.com/doi/pdf/10.1029/2019WR025003),
doi:<https://doi.org/10.1029/2019WR025003>.
URL [https://agupubs.onlinelibrary.wiley.com/doi/abs/10.1029/
670 2019WR025003](https://agupubs.onlinelibrary.wiley.com/doi/abs/10.1029/2019WR025003)
- [63] S. W. Webb, C. K. Ho, Review of enhanced vapor diffusion in porous
media, Tech. rep., United States, sAND-98-1819C (1998).
URL [http://inis.iaea.org/search/search.aspx?orig_q=RN:
30009514](http://inis.iaea.org/search/search.aspx?orig_q=RN:30009514)
- [64] E. Shahraeeni, D. Or, Pore scale mechanisms for enhanced vapor trans-
675 port through partially saturated porous media, *Water Resources Research*
48 (5). arXiv:<https://agupubs.onlinelibrary.wiley.com/doi/pdf/>

10.1029/2011WR011036, doi:<https://doi.org/10.1029/2011WR011036>.

URL <https://agupubs.onlinelibrary.wiley.com/doi/abs/10.1029/2011WR011036>

680

- [65] O. Maalal, M. Prat, D. Lasseux, Pore network model of drying with kelvin effect, *Physics of Fluids* 33 (2) (2021) 027103. arXiv:<https://doi.org/10.1063/5.0035651>, doi:10.1063/5.0035651.

URL <https://doi.org/10.1063/5.0035651>

- 685 [66] Q. Yang, P. Z. Sun, L. Fumagalli, Y. V. Stebunov, S. J. Haigh, Z. W. Zhou, I. V. Grigorieva, F. C. Wang, A. K. Geim, Capillary condensation under atomic-scale confinement, *Nature* 588 (7837) (2020) 250–253. doi:10.1038/s41586-020-2978-1.

URL <https://doi.org/10.1038/s41586-020-2978-1>